Simultaneous Monitoring of Amorphous and Crystalline Phases in Silicalite Precursor Gels. An *In Situ* Hydrothermal and Time-Resolved Small- and Wide-Angle X-ray Scattering Study

By W. H. Dokter, T. P. M. Beelen, H. F. van Garderen and R. A. van Santen

Schuit Institute of Catalysis, University of Technology Eindhoven, PO Box 513, 5600 MB Eindhoven, The Netherlands

W. Bras

NWO, The Hague, The Netherlands, and Daresbury Laboratory, Daresbury, Warrington WA4 4AD, England

and G. E. Derbyshire and G. R. Mant

Daresbury Laboratory, Daresbury, Warrington WA4 4AD, England

Abstract

The gel transformations and subsequent crystallization that occur in the precursor reaction mixture of silicalite were investigated using simultaneous small- and wide-angle X-ray scattering (SAXS–WAXS). The SAXS–WAXS measurements, together with the use of a high flux of synchrotron radiation and a newly developed high-pressure reaction cell, provide the possibility of *in situ* hydrothermal and time-resolved monitoring of amorphous gel transformations and crystallization.

1. Introduction

Zeolites are crystalline amorphous silica–alumina materials that exhibit a combination of properties such as uniform pore dimensions, ion-exchange properties, internal acidity and thermal stability (Bekkum, Flanigan & Jansen, 1991). Owing to these properties, zeolites find wide application in numerous industrial applications, *e.g.* in separation processes, as detergents but mainly as catalysts in heterogeneous catalysis.

Silicalite (Grose & Flanigan, 1977; Flanigan *et al.*, 1978) is a microporous crystalline silica, isostructural with the alumina–silicate zeolite ZSM-5. Silicalite has very small pores, providing a shape-selective molecular sieve interesting for particular catalytic applications. Silicalite can be obtained by hydrothermal treatment (Fegan & Lowe, 1986) of the precursor reaction mixture with tetrapropylammonium ions as templating agent. The perfect silicalite structure does not contain any aluminium ions but, owing to impurities present in the silica source, some aluminium ions will be incorporated in the crystalline structure accompanied by a cation, possibly a proton (Fyfe, Gobbi, Klinowski, Thomas & Ramdas, 1982).

Many investigations have focused on the development of new zeolite types, optimization of crystallization and possible applications for zeolites (*e.g.* Fegan & Lowe, 1986). The underlying molecular mechanisms that lead to a certain type of zeolite are however still poorly understood and only limited knowledge of the transformations occurring in the amorphous gel phase during the induction period is available. After nucleation, the pore structure to be formed in the final product is already present. The gel transformations occurring in the induction period will have to be studied, understood and adjusted, to produce materials with tailor-made properties (pores).

To study the processes preceding the crystallization of the zeolite, *in situ* and noninvasive techniques are desired, preferably providing information about 'structure' present in an amorphous mixture. Techniques like adsorption, mercury porosimetry and transmission/scanning electron microscopy require the removal of pore fluid before analysis (Smith *et al.*, 1992), possibly changing the structure irreversibly, and therefore do not provide appropriate information about the structure present in the wet precursor phase.

Nuclear magnetic resonance (Ginter, Went, Bell & Radke, 1992; Dokter *et al.*, 1993), Raman spectroscopy (Twu, Dutta & Kresge, 1991) and small-angle scattering (X-rays and neutrons) (Bunce, Ramsay & Penfold, 1985; Dokter *et al.*, 1994) can be used to study the precursor gels without altering the structure. Small-angle neutron and X-ray scattering (SANS and SAXS, respectively) provide the advantage that *in situ* measurements under hydrothermal conditions can be performed in special environment cells, developed both for SANS (Dokter *et al.*, 1994) and SAXS (see §2).

Recently, the development of the concept of fractal structures (Mandelbrot, 1979) has provided a very useful tool for interpretation of small-angle scattering

spectra of amorphous gels. Fractal aggregates exhibit the property of self-similarity, meaning that the structure does not change with changing observation length scale within the limits of the aggregate size at large length scales and the primary building-particle size at small length scales. With small-angle scattering, the fractal behaviour and the limits of this behaviour can be determined, providing information about the density gradient present in the sample and the sizes of the primary constructing particles and aggregates (Schaeffer, Martin, Wiltzius & Cannel, 1984). The small-angle scattering spectrum does not change during gelation, that is when the clusters form a percolating network throughout the entire vessel (Cabane, Dubois, Lefaucheux & Robert, 1990).

The relation between a scattering spectrum and the species responsible for the scattering is shown in Figs. 1(a) and (b). For mass fractal aggregates, the scattered intensity will be dominated by the structure factor, providing information about the correlation between the various primary building units present in the aggregates (Martin & Hurd, 1987):

$$I(Q) = N/V \, \Delta\rho \, P(Q)S(Q) \simeq S(Q) \simeq Q^{-D_f}, \qquad (1)$$

where $Q = 2\pi/\lambda \sin(2\Theta)$, λ = wavelength, 2Θ = scattering angle, $\Delta\rho$ = electron-density difference, N = number of scattering entities in irradiated volume V, $P(Q)$ = form factor, $S(Q)$ = structure factor, D_f = mass fractal dimension.

On the scale of the primary building units, the form factor of the primary building units becomes dominant in the scattering pattern, thus providing information about the surface structure of the primary building units (Bale & Schmidt, 1983):

$$I(Q) \simeq P(Q) \simeq Q^{-(6-D_s)}, \qquad (2)$$

with D_s being the surface fractal dimension, ranging between 2 and 3. The surface fractal dimension equals
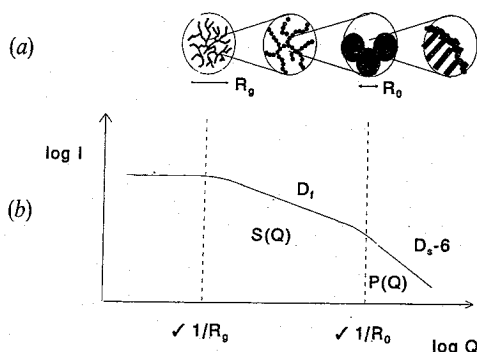

Fig. 1. Schematic representation of (a) an aggregate with mass fractal and surface fractal properties and (b) the matching small-angle scattering spectrum, with $S(Q)$ = structure factor, $P(Q)$ = form factor, I = scattered intensity, Q = scattering vector, D_f = mass fractal dimension, D_s = surface fractal dimension, R_g = radius of gyration of the aggregate and R_0 = radius of gyration of primary particles.

2 for a nonfractal completely smooth surface, resulting in the well known Porod (1951) relation:

$$I(Q) \simeq Q^{-4}. \qquad (3)$$

If D_s increases, the roughness of the surface will increase. When $D_s \rightarrow 3$ and $D_f \rightarrow 3$, then a homogeneous distribution of mass and voids (possibly filled) throughout the sample is obtained (Schaeffer & Hurd, 1990).

Experimentally, the parameter D (fractal dimension) can be determined from a plot on which $\log I(Q)$ is drawn as a function of $\log Q$. The slope of the scattering curve, α, is equivalent to D_f for mass fractal scattering and equivalent to $-(6 - D_s)$ for surface fractal scattering.

Gel transformations occurring during the induction period can be monitored with SAXS while crystallinity can be monitored with WAXS. Combination of both these techniques provides a very powerful tool for the investigation of the transformations in the gel phase (leading or not leading to crystalline zeolite materials) and the crystallinity of the zeolite simultaneously.

X-ray diffraction experiments performed with conventional equipment suffer from the problem that the data-collection times are relatively long even when a rotating-anode generator is used in combination with a position-sensitive detector. This is a hindrance when samples have to be studied in which the time scale of a single diffraction experiment is not compatible with the time scale of the evolution of the sample, as for the silicalite synthesis described here and by Dokter *et al.* (1994). Furthermore, problems occur concerning sample change proceeding from the wet environment of the reaction cell to the dry and ambient environment of the diffraction apparatus. By use of a synchrotron-radiation beam line, these problems can easily be overcome. Moreover, owing to the intrinsic low divergence and high collimation of synchrotron radiation, it is possible to conduct simultaneous SAXS and WAXS experiments on a suitably adapted beamline.

We have used a recently developed instrument at the Synchrotron Radiation Source (Daresbury) for combined SAXS–WAXS experiments on the synthesis of silicalite under hydrothermal conditions. A new sample cell was constructed that enabled us to control the pressure and temperature of the sample. In this paper, the results of the synthesis of silicalite under hydrothermal conditions studied with the above-described SAXS–WAXS equipment are presented and discussed.

2. Experimental

SAXS–WAXS

The SAXS–WAXS experiments were performed on beam line 8.2 of the SRS at Daresbury. In this section,

the experimental set-up with respect to the SAXS–WAXS experiments is described (Fig. 2). The length of the vacuum chamber is 3.5 m. The Q range covered with SAXS is $0.01 < Q < 0.175 \, \text{Å}^{-1}$ and the Q range covered with WAXS is $0.8 < Q < 3.4 \, \text{Å}^{-1}$. The wavelength λ of the X-rays is $1.5 \, \text{Å}$ and $\Delta\lambda/\lambda < 4 \times 10^{-3}$. More details concerning camera geometry and data collection have been presented extensively elsewhere (Bras et al., 1993).

When hydrothermal experiments are performed at elevated temperatures, care has to be taken that no water is lost from the sample by cell leakage. Therefore, a sealed sample chamber was constructed that could be both temperature and pressure controlled. The actual brass reaction cell was placed in this chamber and was temperature controlled with the help of a resistance heater and a proportional integration derivative (PID) controller. The sample chamber was pressurized with dry nitrogen to the vapour pressure of water at the relevant temperature. In this way, the mica windows of the sealed reaction cell are not subject to a pressure differential and consequently the water does not evaporate from the sample. The pressurized chamber and reaction cell were constructed such that the X-ray path length was minimized in order to reduce absorption and background scattering. The sample chamber was separated from the camera vacuum by a $125 \, \mu\text{m}$ Kapton window.

The temperature during the experiment was carefully increased to reaction temperature in approximately 20 min to 463 K. The temperature was monitored using a thermocouple, which was placed near the sample. Off-line tests showed that the temperature could be controlled with an accuracy of ± 5 K. During the heating of the reaction cell, the pressure in the chamber surrounding the cell was carefully and simultaneously increased to 3×10^5 Pa N_2 at the final reaction temperature.

The SAXS pattern is detected with a standard Daresbury quadrant detector (Lewis et al., 1992) located 3.5 m from the sample position. A beam stop is mounted before the SAXS exit window, to prevent the direct beam from hitting the SAXS detector. The quadrant detector has an advantage over linear

detectors in that the active area increases radially. This improves the signal-to-noise ratio at larger scattering angles where the scattered intensity is lowest. The spatial resolution of the SAXS detector is $400 \, \mu\text{m}$ and it can handle up to 3×10^5 counts s^{-1}. The WAXS detector is a curved knife-edge Inel detector (Evain, Deniard, Jouanneaux & Brec, 1993) with a spatial resolution of $50 \, \mu\text{m}$ and can handle up to 10^5 counts s^{-1}. It can cover $120°$ of arc at a radius of 0.2 m but only $90°$ of arc are used in these experiments.

When the slope of the scattering curve is determined, two possible sources of error may be distinguished. The first is the natural noise present in the data, which is, however, small compared with the error introduced during background subtraction. To correct for the background signal, the procedure introduced by Vonk (1973) was used. The error introduced during this procedure is larger than all other errors and is indicated in Fig. 5 by error bars.

The Q axis of the SAXS pattern was calibrated with an oriented specimen of wet rat-tail collagen. A fully crystallized specimen of zeolite A (NaA, Procter and Gamble) was used to calibrate the Q axis of the WAXS pattern. The incident intensity was recorded by a parallel-plate ionization detector. Appropriate attenuators were used in order not to exceed the data rates that both detectors can handle. The experimental data were corrected for background scattering, sample thickness, and transmission and detector sensitivity.

Materials

Zeolite precursor mixtures were prepared using Aerosil 380 (Degussa AG) as a silica source. Appropriate amounts of sodium hydroxide (Merck p.a.) and water (double demineralized) were added as well as the template tetrapropylammonium bromide (TPA) (Aldrich Chemie 98%), in the following ratios: $SiO_2/TPA = 6.25$, $SiO_2/NaOH = 12.8$ and $H_2O/SiO_2 = 13.8$ (El Hage-Al Asswad et al., 1988). The sodium hydroxide and tetrapropylammonium bromide were dissolved in water. Then the silica was added and stirred until a smooth slurry with a uniform consistency was obtained. The reaction mixture was immediately transferred to the reaction cell. Experiments were carried out under nonstirred conditions at a temperature of approximately 463 K.

X-ray diffraction

The X-ray diffraction (XRD) spectra were recorded on a Philips PW 7200 diffractometer using Cu $K\alpha$ radiation. Measurements were performed between 5 and $70°$ with a scan rate of $2° \, \text{min}^{-1}$. The crystallinity of the final product was determined with XRD, which was calibrated with a fully crystallized sample of silicalite.
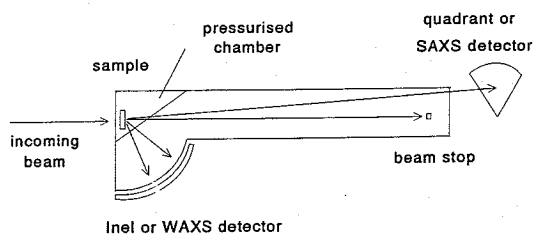

Fig. 2. Schematic representation of the experimental SAXS–WAXS set-up.

3. Results and discussion

In Fig. 3, the SAXS spectra (Figs. 3*a* and *b*) and a three-dimensional plot of the WAXS spectra (Fig. 3*c*) of the synthesis of silicalite are shown as a function of time. For clarity, not all the SAXS spectra have been shown. The slopes α, calculated with a least-squares fit from the log–log plots from the SAXS spectra in the range $-0.7 < \log Q < -1.6 \text{ Å}^{-1}$, range between -3.4 and -4. With reference to (1) to (3), it is obvious that the amorphous precursor system exhibits surface fractal behaviour $(2 < D_s < 2.6)$. The power-law behaviour of the scattering extends over approximately one decade. Unlike in SANS experiments reported elsewhere (Dokter *et al.*, 1994), no radius of gyration of amorphous zeolite particles could be derived from the SAXS spectra. For experimental reasons, the accessible Q range is not exactly the same in the two different experiments. The value found for the surface fractal dimension for the starting reaction mixture, $D_s = 6 + \alpha = 2.7$, is, within the experimental error, equal to the value previously found with SANS (2.6). This value is indicative of a very rough surface structure.

SANS experiments performed at elevated temperatures (Dokter *et al.*, 1994), on the same synthesis mixtures as used in this study, showed a displacement of the scattering pattern to smaller Q values and a decrease of the surface fractal dimension from 2.7 to 2.25 (at 403, 423, 443 and 463 K). The particle size of the unreacted precursor mixture was approximately 140 Å and increased as a function of reaction time. At higher temperatures (443, 463 K), these particles grow rapidly but, at lower temperatures, larger sizes are obtained. Particles grow and are smoothed by addition of amorphous material from the amorphous bulk. Growth is observed both before as well as after crystallization is started, indicating that the crystallization starts in or on the growing amorphous gel particles.

The decrease of the surface fractal dimension is also observed in the SAXS pattern obtained at 463 K. The values of the surface fractal dimension as found with SAXS are smaller than the values found in the SANS experiment. No significant displacement in the SAXS spectra as a function of time is observed when the spectra are plotted in one figure [the spectra in Figs. 3(*a*) and (*b*) have been shifted for clarification]. This
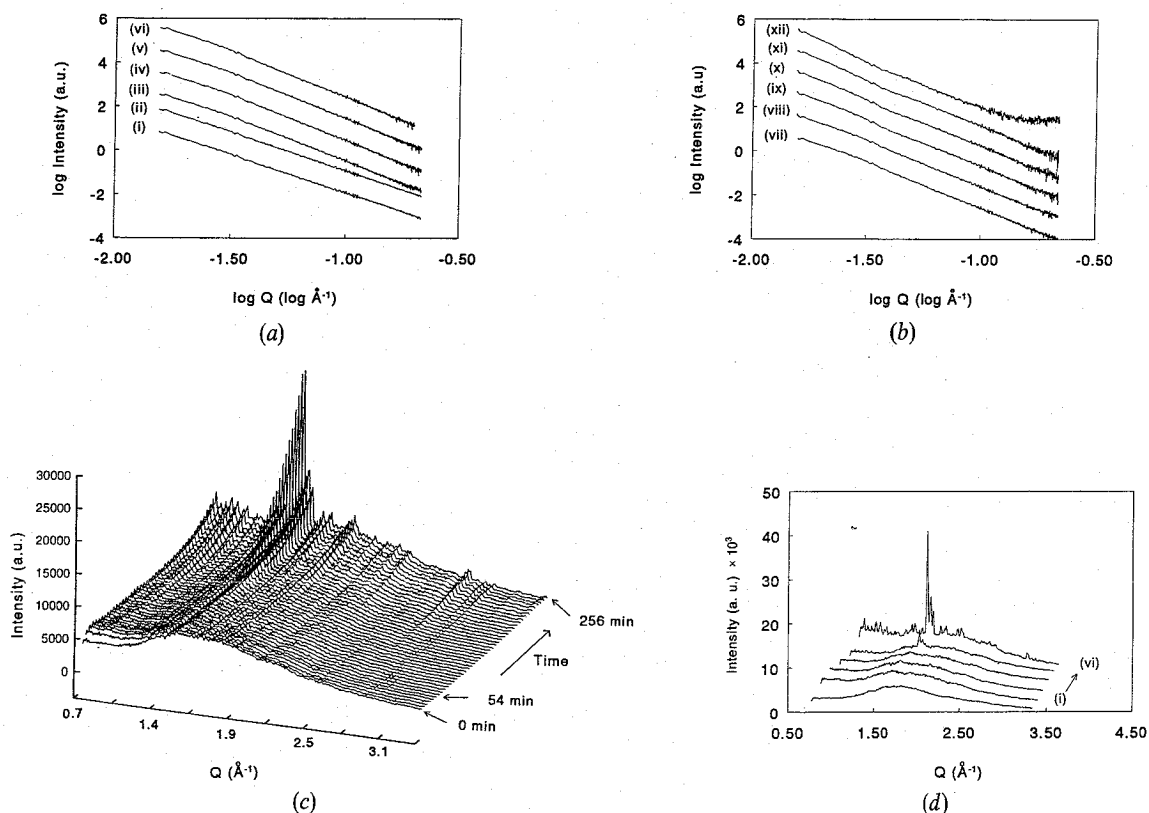

(a)

(b)

(c)

(d)

Fig. 3. (*a*), (*b*) Small-angle X-ray scattering spectra during silicalite synthesis performed at 463 K at various times: (i) 0, (ii) 10, (iii) 20, (iv) 32, (v) 41, (vi) 48, (vii) 54, (viii) 61, (ix) 106, (x) 156, (xi) 206 and (xii) 256 min. The spectra have been shifted for clarification. (*c*) Three-dimensional representation of the WAXS spectra as a function of time during silicalite synthesis performed at 463 K between 0 and 256 min reaction time. (*d*) Three-dimensional representation of a number of relevant WAXS spectra in order to demonstrate clearly the onset of crystallization [(*c*)]. The spectra have been shifted for clarification. The intensity is expressed in arbitrary units (a.u.).

might be explained by the increased number of amorphous gel particles that will be formed at higher temperatures compared with reactions performed at lower temperatures. The size of the amorphous particles does not change throughout the induction period nor in the subsequent crystallization period, which might be indicative of the nucleation of the zeolite crystals in or on the amorphous gel particles. After approximately 50 min reaction, no changes in surface roughness are observed while the crystallinity is increasing. This implies that the electron scattering density of the reorganized amorphous particles is equal to the electron scattering density of the zeolite crystals.

The WAXS spectra shown in Fig. 3(*d*) indicate no signs of crystallinity after short reaction times. The bump observed at approximately $2\Theta = 26°$ is due to amorphous scattering from water present in the reaction mixture. Crystallization of silicalite starts after 54 min of reaction, as can be observed in the WAXS spectra (Fig. 3) where a peak at $2\Theta = 23.2°$ starts to grow. This is known to be the most intense peak in the diffraction pattern of silicalite (von Ballmoos, 1984). Unfortunately, two other very intense peaks in the XRD pattern of silicalite ($2\Theta = 7.9$ and $8.9°$) cannot be observed owing to the small data gap between the two detectors. The peaks grow gradually and after 256 min the maximum crystallinity is reached. After prolonged reaction times, the intensity of the diffraction peaks and the SAXS signal decreased owing to sedimentation of the zeolite crystals in the reaction cell.

In Fig. 4, the diffraction spectra of the final product, measured both with the SAXS–WAXS set-up (WAXS) and with a standard diffraction apparatus (XRD), are compared. The peaks of the XRD spectrum are better resolved than the peaks obtained by WAXS, owing to the limited number of data points (maximum 512) available on the Inel–WAXS detector. The WAXS spectrum shown was recorded in 5 min while the XRD

spectrum was obtained in 30 min over the same angular range. The signal-to-noise ratio in the WAXS spectra is sufficient after 1 min of data collection but the accumulation time was set to 5 min to obtain an adequate signal-to-noise ratio for the SAXS spectrum. The differences in intensity of the WAXS diffraction peaks compared with the XRD ones is due to the above-described limited number of data points in the WAXS spectrum, which causes peaks close in scattering angle to coincide.

The crystallinity percentage is determined from the intensity of the three most intense peaks of the final product divided by the intensity of the same three peaks in the preceding samples. In Fig. 5, the progress of crystallinity is plotted together with the progress of the surface fractal dimension as a function of time. The crystallinity determined from the WAXS spectra was normalized with the help of the XRD spectrum. The crystallinity was found to be approximately 85% for the final product.

It can be seen that the crystallization starts after the surface roughness of the zeolite particles is constant as a function of time (surface fractal dimension constant; see Fig. 5). This implies the need for a reorganization of the amorphous gel phase before crystallization can take place or a reorganization in the precursor phase during which crystallization nuclei are formed. In the latter case, however, these nuclei are too small to be observed by WAXS.

4. Concluding remarks

Results obtained with earlier SANS experiments on the synthesis of silicalite are confirmed by the SAXS results of the combined SAXS–WAXS experiment. Important information can be obtained from the simultaneously obtained WAXS data.

With the combined SAXS–WAXS equipment, it is possible to obtain very useful information concerning the mechanism by which zeolite precursor mixtures transform during synthesis in the amorphous phase as well as in the subsequent crystalline phase. This
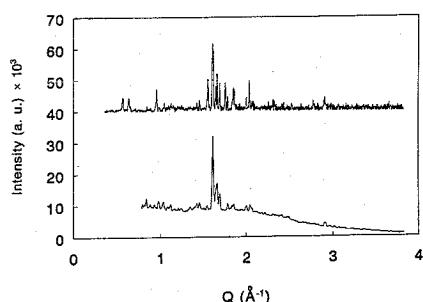

Fig. 4. Diffraction spectra of the final state of the silicalite synthesis performed with the SAXS–WAXS set-up. The top curve is the diffraction spectrum produced with the standard apparatus. The bottom curve is the diffraction spectrum produced with the SAXS–WAXS equipment.
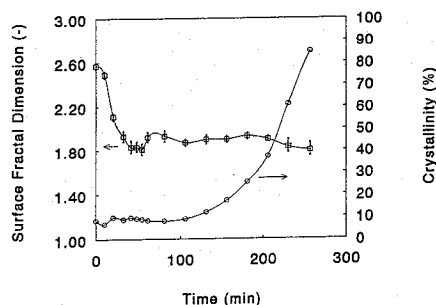

Fig. 5. The development of the surface fractal dimension and the crystallinity during the synthesis of silicalite at 463 K as a function of time.

experimental technique, combined with the newly developed high-pressure reaction cell, also provides the possibility to perform time-resolved experiments while the sample is subjected to elevated temperatures and high pressure (*i.e.* hydrothermal conditions). In this way, it is possible to emulate practical industrial processing conditions and to obtain information over a wide range of length scales. The information content of the experiments is large. Problems concerning changes occurring in the sample proceeding from the hydrothermal reaction cell to the dried and ambient sample cell of the diffraction apparatus are avoided.

The application of the combination of these techniques can elucidate the reaction paths of the synthesis of materials, as is demonstrated by the on-line synthesis of silicalite, and provides exciting new possibilities for material science research.

References

BALE, H. D. & SCHMIDT, P. W. (1983). *Phys. Rev. Lett.* **53**, 596–599.

BALLMOOS, R. VON (1984). *Collection of Simulated XRD Powder Patterns for Zeolites.* Guildford: Butterworth Scientific Limited.

BEKKUM, H. VAN, FLANIGAN, E. M. & JANSEN, J. C. (1991). Editors. *Introduction to Zeolite Science and Practice.* Amsterdam: Elsevier.

BRAS, W., DERBYSHIRE, G. E., RYAN, A. J., MANT, G. R., FELTON, A., LEWIS, R. A., HALL, C. J. & GREAVES, G. N. (1993). *Nucl. Instrum. Methods Phys. Res.* A**326**, 587–591.

BUNCE, J., RAMSAY, J. D. F. & PENFOLD, J. (1985). *J. Chem. Soc. Faraday Trans.* 1, **81**, 2845–2854.

CABANE, B., DUBOIS, M., LEFAUCHEUX, F. & ROBERT, M. C. (1990). *J. Non-Cryst. Solids*, **119**, 121–131.

DOKTER, W. H., BEELEN, T. P. M., VAN GARDEREN, H. F., RUMMENS, C. P. J., VAN SANTEN, R. A. & RAMSAY, J. D. F. (1994). *Colloids Surf. A.* In the press.

DOKTER, W. H., VAN GARDEREN, H. F., BEELEN, T. P. M., DE HAAN, J. W., VAN DE VEN, L. J. M. & VAN SANTEN, R. A. (1993). *Colloids Surf. A*, **72**, 165–171.

EL HAGE-AL ASSWAD, J., DEWAELE, N., NAGY, J. B., HUBERT, R. A., GABELICA, Z., DEROUANE, E. G., CREA, F., AIELLO, R. & NASTRO, A. (1988). *Zeolites*, **8**, 221–227.

EVAIN, M., DENIARD, P., JOUANNEAUX, A. & BREC, R. (1993). *J. Appl. Cryst.* **26**, 563–569.

FEGAN, S. G. & LOWE, B. M. (1986). *J. Chem. Soc. Faraday Trans.* 1, **82**, 785–799.

FLANIGAN, E. M., BENNET, J. M., GROSE, R. W., COHEN, J. P., PATTON, R. L., KIRCHNER, R. M. & SMITH, J. V. (1978). *Nature (London)*, **271**, 512–516.

FYFE, G. A., GOBBI, G. C., KLINOWSKI, J., THOMAS, J. M. & RAMDAS, S. (1982). *Nature (London)*, **296**, 530–533.

GINTER, D. M., WENT, G. T., BELL, A. T. & RADKE, C. J. (1992). *Zeolites*, **12**, 733–741, 742–749.

GROSE, R. W. & FLANIGAN, E. M. (1977). US Patent No. 4 061 724.

LEWIS, R. A., FORE, N. S., HELSBY, W., HALL, C., JONES, A., PARKER, B., SUMNER, I., WORGAN, J. S. & BUDTZ-JORGENSEN, C. (1992). *Rev. Sci. Instrum.* **63**(1), 642–647.

MANDELBROT, B. B. (1979). *The Fractal Geometry of Nature.* San Francisco: Freeman.

MARTIN, J. E. & HURD, A. J. (1987). *J. Appl. Cryst.* **20**, 61–78.

POROD, G. (1951). *Kolloid Z.* **124**, 83–87.

SCHAEFFER, D. W. & HURD, A. J. (1990). *Aerosol Sci. Technol.* **12**, 876–890.

SCHAEFFER, D. W., MARTIN, J. E., WILTZIUS, P. & CANNEL, D. S. (1984). *Phys. Rev. Lett.* **52**, 2371–2374.

SMITH, D. M., DESHPANDE, R., BRINKER, C. J., EARL, W. L., EWING, B. & DAVIS, P. J. (1992). *Catal. Today*, **14**, 293–303.

TWU, J., DUTTA, P. K. & KRESGE, C. T. (1991). *Zeolites*, **11**, 672–679.

VONK, C. G. (1973). *J. Appl. Cryst.* **6**, 81–86.